ELSEVIER

Journal of Power Sources 112 (2002) 199–208

JOURNAL OF POWER SOURCES

www.elsevier.com/locate/jpowsour

Effect of Sn and Ca doping on the corrosion of Pb anodes in lead acid batteries

Dragan Slavkov[a], Bala S. Haran[a], Branko N. Popov[a,*], Frank Fleming[b]

[a]*Center of Electrochemical Engineering, Department of Chemical Engineering, University of South Carolina, Columbia, SC 29208, USA*
[b]*NorthStar Battery Company, 2005-T East Kearney Street, Springfield, MO 65803, USA*

Received 13 June 2002; accepted 24 June 2002

Abstract

Doping with Sn and Ca is seen to improve the reversibility and charging efficiency of lead anodes used in lead acid batteries. However, one drawback of these materials is their increased corrosion rate as compared to pure lead anodes. In the present investigation, the dissolution of Pb–Sn and Pb–Sn–Ca alloys has been evaluated under different float charge conditions for extended periods of time. The float potential has been optimized based on minimum anode dissolution and oxygen evolution. Extended cycling studies show that doping with Sn maintains the reversibility of the anode. In order to minimize the weight of the anode, a small amount of Sn was coated on Pb by electrodeposition. The coated electrode reveals similar reversibility and dissolution characteristics as the Sn doped anode. Electrodeposition is seen to offer an inexpensive route for increasing the charging efficiency of Pb anodes in lead acid cells without increasing the weight of the battery.
© 2002 Elsevier Science B.V. All rights reserved.

Keywords: Corrosion; Pb anodes; Lead acid batteries; Doping tin; Calcium

1. Introduction

The shift to maintenance free batteries has resulted in the search for non-antimonial grid compositions in lead acid batteries. The initial approach to solve this problem has been to use pure lead anodes or lead calcium binaries. The use of pure lead gives rise to a strong oxide passive layer formation at the grid/active-material interface [1,2]. This oxide layer is highly stable in the acidic environment present in lead acid batteries. The insulating passive film reduces the anode dissolution thereby increasing the active life of the battery [3]. However, this also has an undesirable effect of increasing the impedance of the anode after storage for a certain period of time. The increased resistance reduces the reversibility and charging efficiency during subsequent cycles [4]. Similar difficulties have also been observed from cells that have been deep discharged [5]. Several studies have looked at the nature of the passive film formed on the anode. The composition of the passive layer is a mixture of $PbSO_4/PbO_x$ ($1 < x < 2$) [6]. On the surface of the lead grid tetragonal-PbO is formed, which acts as an insulator toward current flow. On the surface of tet-PbO, different forms of PbO_2 are formed. Above this $PbSO_4$ or mixed sulfate deposits are formed. The layers of PbO_2 and $PbSO_4$ are semi-permeable in nature and allow selective transport of ionic species. The cumulative effect of these different oxide and sulfate layers is to prevent electron and ionic flow thereby preventing reversible cycling of the anode [3–5]. The formation of a thick oxide film is prevented in antimony based lead grids due to the solubility of different antimony sulfate species formed. In order to improve electrode performance different dopants have been studied to improve the dissolution of the passive film. Among these incorporation of Sn even at levels of 0.5 wt.% improves the reversibility of the anode both after storage and deep discharge [6,7].

The effect of Sn doping on grid passivation has been studied in detail. According to Giess [8], tin suppresses the transformation of lead to α-PbO. Similar conclusions were derived by Pavlov et al. [9] who suggested that Sn is incorporated into the PbO/PbO_x crystal lattice. According to Takahashi et al. [10] tin accelerates the growth of α-PbO_2 which prevents the formation of a $PbSO_4$ layer on the surface of the grid. However, Carter et al. [11] found that lead–calcium–tin anodes lost 20% of their initial capacity after 50 cycles of deep discharge. The observed decline in capacity was attributed to the loss in contact between the grid and the active material and due to increase in the rate of surface

* Corresponding author. Tel.: +1-803-777-4181; fax: +1-803-777-8265.
E-mail address: popov@engr.sc.edu (B.N. Popov).

0378-7753/02/$ – see front matter © 2002 Elsevier Science B.V. All rights reserved.
PII: S0378-7753(02)00368-3

product formation. Nelson and Wisdom [12] found that addition of Sn leads to the formation of discontinuous oxide layers on plates during float charge. They also found that Pb–Sn alloys exhibited increased corrosive attack along the grain boundaries at grid–electrolyte interface. As seen from the review of the literature [8–12] addition of Sn leads to increased reversibility and superior charge acceptance. However, it also leads to increased loss of active material due to dissolution of the passive film [11].

Corrosion of positive grids with Sn in lead acid cells will proceed continuously during float charge and shorten the lifetime of the battery. The rate of corrosion can be minimized by varying the float potential. Also, a review of the mechanism of alloy passivation indicates that the poor reversibility is associated with the surface oxides formed rather than on the bulk of the anode. Hence the objectives of this study were two-fold: the first objective was to determine the corrosion rate of Pb–Sn (0.6%) and Pb–Sn (1.1%)–Ca (0.03%) alloys in 30% sulfuric acid solution under different applied float potentials. The reversibility of these alloys under various potential scans has also been studied. Next, Sn was electrodeposited on the surface of lead and the reversibility and dissolution characteristics were studied. The characteristics of Sn coated and Sn doped anodes were compared. Electrochemical and material characterization were done to determine the extent of alloy corrosion and the nature of the surface film formed.

2. Experimental

Lead plates from NorthStar were cut into samples of 2 in. × 2 in. dimension. Two different alloys were studied Pb–Sn (0.6%) and Pb–Sn (1.1%)–Ca (0.03%). The plates were subsequently degreased with acetone and polished and washed with demineralized water. Two set of studies were done: (i) short range electrochemical studies and (ii) long range dissolution studies. A three-electrode setup was used to study the electrochemical behavior of Pb alloys. The electrolyte used in this study is 30% sulfuric acid with 10 g/l sodium sulfite. Lead grids of Pb–Sn (1.1%) were used as the counter electrode. Hg/Hg_2SO_4 was used as the reference electrode. All potentials in this study are referred with respect to the Hg/Hg_2SO_4 electrode. Electrochemical studies were done using Scribner Associated Corrware Software with EG&G Princeton applied model 273 potentiostat/galvanostat and a Solartron 1255 frequency analyzer. The sample was left on open circuit until its potential stabilized. After the potential stabilized, non-destructive evaluation of the surface was done using linear polarization and impedance analysis. During linear polarization, the potential was varied 10 mV above and below the open circuit potential of the mineralized sample at a scan rate of 1 mV/s. The impedance data generally covered a frequency range from 5 mHz to 10 kHz. A sinusoidal ac voltage signal varying by ±10 mV was applied. The electrode was stable during the experiments and its open circuit potential changed less than 1 mV. The variation of the corrosion potential of the samples was measured with time. Apart from this, cyclic polarization, cyclic voltammetry and potentiostatic polarization studies were done on the different Sn alloys.

Separately, samples of Pb–Sn and Pb–Sn–Ca alloy were kept in 30% sulfuric acid solution for the long range dissolution studies. The samples were polarized to 1.2, 1.22, 1.25, 1.3 and 1.35 V with respect to the Hg/Hg_2SO_4 electrode and the corrosion current was recorded as a function of time. After the test period of 6 weeks, the samples were removed, washed with DI water and the weight loss was determined. All studies were conducted at a temperature of 25 °C. The sample size for all studies was 8 $in.^2$ or 51.61 cm^2.

Electrodeposition of Sn on lead was done using a two electrode setup. Lead plate was used as the working electrode and platinized titanium served as the counter electrode. Deposition was done in 200 g/l $Sn(BF_4)_2$ + 100 g/l HBF_4 at a constant voltage of 3 V for different periods of time. The deposit thickness varied between 500 and 800 μm. Subsequent to deposition the anode was characterized electrochemically in a similar manner as the Pb–Sn and Pb–Sn–Ca alloys. Changes in the alloy surface due to electrodeposition and corrosion were studied using energy dispersive spectroscopy (EDAX) and scanning electron microscopy (SEM).

3. Results and discussions

3.1. Pitting tendency of Pb–Sn and Pb–Sn–Ca alloys

Cyclic polarization gives an indication of the extent of pitting of the lead sample. Fig. 1 presents the cyclic polarization plot of the lead–Sn (0.6%) alloy. The potential has been scanned from −1.2 to +0.5 V and then back to −1.2 V. On shifting the potential to more positive values, a reduction

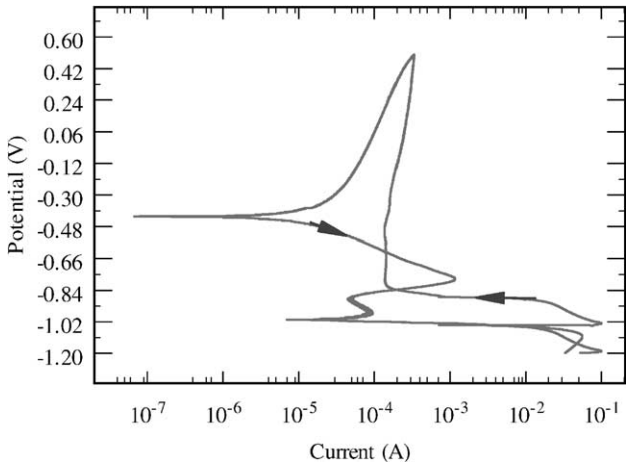

Fig. 1. Cyclic polarization plot of Pb–Sn (0.6%) alloy in 30% sulfuric acid. In all studies, lead grids of Pb–Sn (1.1%) were used as the counter electrode and Hg/Hg_2SO_4 was used as the reference electrode.

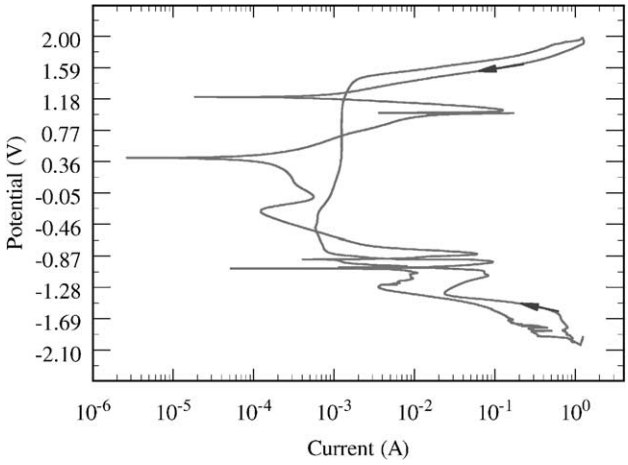

Fig. 2. Cyclic polarization plot of Pb–Sn alloy covering the potential range of −1.93 to +1.98 V.

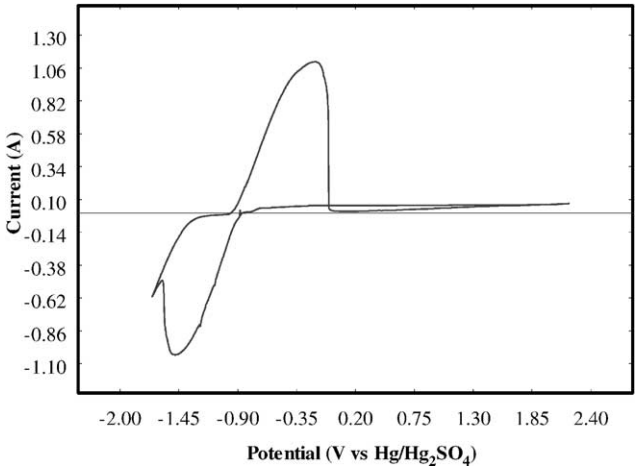

Fig. 3. Cyclic voltammograms for pure Sn in 30% sulfuric acid solution. The potential was swept at a scan rate of 25 mV/s between −1.7 and 2.0 V.

in current corresponding to the lead/lead sulfate negative electrode is seen at −1 V. Increasing the potential further leads to passivation of the sample. This is associated with the formation of PbO on the surface of lead.

Fig. 2 presents the cyclic polarization of the same sample for the potential range of −1.93 to +1.98 V. This has been done to determine the pitting tendency of the Pb–Sn alloy. Pitting corrosion is a highly localized form of corrosion occurring on a metal surface. Pitting is commonly observed on surfaces with little or no general corrosion. Pitting typically occurs as a process of local anodic dissolution where metal loss is exacerbated by the presence of a small anode and a large cathode. During cyclic polarization test the potential is swept in the anodic direction until localized corrosion initiates as indicated by a large increase in the applied current. This occurs at approximately 1.5 V in Fig. 2. At this point, the direction of the scan is reversed, and the current decreases until it changes polarity. E_{bd} (the breakdown potential) is the potential above which pits are initiated, while E_{rp} (the repassivation potential) is the potential below which pits repassivate. The breakdown potential is usually defined as the potential at which there is a large increase in the applied current, while the repassivation potential is the potential on the reverse scan at which the applied anodic current becomes zero (i.e. the current changes polarity). From Fig. 2 it can be seen that the repassivation potential is around +1.2 V which corresponds to the $PbO_2/PbSO_4$ couple. The higher value of E_{bd}, indicates that the alloys is more resistant to the initiation of localized attack. Also, since E_{rp} is large and close to E_{bd}, the alloy can repassivate easily. At potentials between E_{rp} and E_{bd}, sites that have initiated can propagate. In general, the larger the hysteresis, the more likely a localized corrosion site will propagate once initiated. In this case, the breakdown potential is close to the repassivation potential and the hysteresis is very small. Similar behavior is also seen for the lead–Sn–Ca alloy. These studies indicate that doping with Sn and Ca does not lead to aggressive pitting attack in the sulfuric acid electrolyte.

3.2. Studies on alloy reversibility

The reversibility of the Pb–Sn and Pb–Sn–Ca alloys can be studied using cyclic voltammetry. Fig. 3 shows the voltammograms for pure Sn between the potential range −1.7 to 2.0 V. Increasing the potential to more positive values from −1.7 V, it is seen that Sn is oxidized. Tin is stable in dilute acids and does not react with either dilute hydrochloric acid or dilute sulfuric acid at room temperature. However, in strong acids Sn undergoes oxidation, which is seen by the peak observed at −0.35 V. Increasing the potential to more positive values leads to a decrease in oxidation current. This indicates that the tin oxide formed on the surface prevents further dissolution of Sn. Reversing the potential leads to reduction of oxides and a peak is observed at −1.5 V. As seen in Fig. 2, the $PbO_2/PbSO_4$ couple has an equilibrium potential around 1.2 V. At this potential a small oxidation current is seen in Fig. 3 indicating that Sn is inert in the potential range of 0.2–2.0 V.

Fig. 4 shows CVs of the Pb–Sn–Ca alloy at a scan rate of 25 mV/s. The alloy was cycled between 0.65 and 1.35 V. Initially (Fig. 4a) no peaks are seen in the forward scan (0.6–1.3 V). Beyond 1.3 V, a large increase in current is seen. Since Sn is inert in this potential range, this corresponds to formation of PbO_2 and oxygen evolution. On the reverse sweep, a large peak appears close to 1.07 V. This can be attributed to the conversion of PbO and PbO_2 on the surface to $PbSO_4$. After activating the sample for five cycles, CVs were continued at the same scan rate of 25 mV/s in the potential range of 0.6–1.3 V. These CVs are shown in Fig. 4b. In this case, a peak is seen in the forward scan also. This corresponds to the formation of PbO_2. In the first cycle the maximum in the oxidation peak is seen at 1.175 V. Subsequently this peak shifts slightly to more negative values and

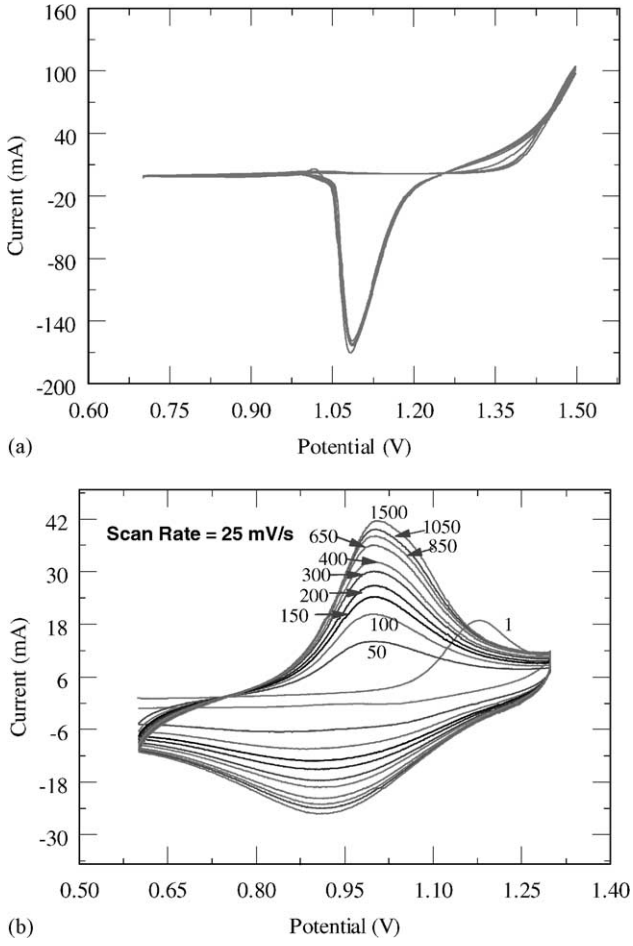

Fig. 4. Cyclic voltammograms of the Pb–Sn–Ca alloy at a scan rate of 25 mV/s. (a) Initial cycling between 0.65 and 1.35 V and (b) after five cycles between 0.6 and 1.3 V.

appears at 1.0 V. A characteristic feature of the CVs is the continuous increase in the oxidation and reduction currents with cycling. This indicates that more amount of Pb is converted to PbO_2 and $PbSO_4$ with cycling.

Similar behavior is seen for the Pb–Sn alloy also in the potential range 0.6–1.25 V (Fig. 5). In this case, the oxidation current at any given cycle is much smaller than that seen

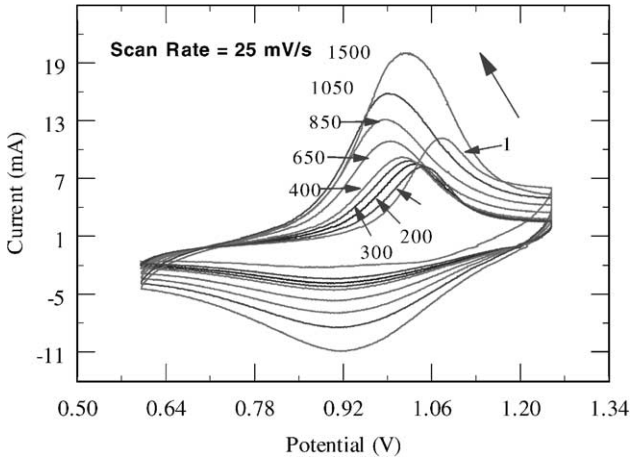

Fig. 5. Cyclic voltammograms of the Pb–Sn alloy at a scan rate of 25 mV/s. The electrode was initially activated by cycling between 0.65 and 1.35 V for five times.

for the Pb–Sn–Ca alloy. This can be attributed to the lower Sn content in this alloy. However, beyond the first cycle, for both alloys the potential at which the peak oxidation and reduction current appears does not change. This indicates that a stable potential for $PbO_2/PbSO_4$ is established which does not change with cycling. Since the goal of this study is to investigate the effect of polarization on corrosion characteristics, it is essential to establish the reversible potential for PbO_2–$PbSO_4$ couple for both alloys. Table 1 presents the peak oxidation current and potential for both alloys. In addition, we also present the potential at which the current polarity changes, i.e. $E_{rev,f}$ corresponds to the potential at which the current in the forward sweep (0.6 to 1.25/1.30 V) becomes positive and $E_{rev,b}$ corresponds to the potential at which the current in the reverse sweep (1.25/1.30 to 0.6 V) becomes negative.

From Table 1, it is clear that the oxidation peak potential changes less than 60 mV for the Pb–Sn alloy and less than 20 mV for the Pb–Sn–Ca alloy. The peak oxidation current increases with cycling for both alloys. However, the rate of increase decreases with cycling for the Pb–Sn–Ca alloy. For example, the peak current increases 48% for the Pb–Sn–Ca

Table 1
Change in peak current, peak potential and reversible potential for Pb alloys

Cycle number	Peak current (mA)		Peak potential (V)		$E_{rev,f}$ (V)		$E_{rev,b}$ (V)	
	Pb–Sn	Pb–Sn–Ca	Pb–Sn	Pb–Sn–Ca	Pb–Sn	Pb–Sn–Ca	Pb–Sn	Pb–Sn–Ca
1	11.18	18.93	1.075	1.179	0.743	–	1.133	1.050
50	8.21	14.09	1.055	1.008	0.731	0.683	1.186	1.176
100	8.21	20.30	1.049	0.992	0.729	0.694	1.195	1.208
200	8.51	26.90	1.035	1.003	0.725	0.703	1.203	1.227
300	8.83	30.00	1.024	0.993	0.719	0.707	1.202	1.233
400	9.19	32.30	1.011	1.000	0.715	0.710	1.201	1.238
650	10.87	36.10	0.996	0.995	0.709	0.711	1.200	1.242
850	13.04	38.20	0.993	1.004	0.709	0.717	1.198	1.244
1050	15.83	39.70	0.992	1.002	0.712	0.719	1.200	1.246
1500	20.00	41.60	1.011	1.001	0.729	0.718	1.210	1.248

alloy between 100 and 300 cycles. However, between cycles 1050 and 1500 the increase is only 4.8%. However, a similar trend is not seen for the Pb–Sn alloy. For example, the peak current increases 7.55% between cycles 100 and 300 and 26.3% between cycles 1050 and 1500. This is in opposite to that seen for pure lead where the oxidation current decreases with cycling [6]. These results clearly show that addition of Sn aids in dissolution of the passive film and increases the reversibility of the anodic reaction. The last column in Table 1 presents the potential at which current becomes negative during the reverse sweep. This corresponds to the reduction of PbO_2 to $PbSO_4$. This potential is around 1.2 V for the Pb–Sn alloy and 1.24 V for the Pb–Sn–Ca alloy. When applying a float voltage to the positive electrode, in order to keep it in the oxidized state the value should be more positive than 1.2/1.24 V.

3.3. Alloy dissolution studies at different float potentials

Fig. 6a shows the dissolution rate of Pb–Sn alloy under potentiostatic conditions. Beyond 25 h no change in the corrosion current with time is seen. The studies were done for a time of 6 weeks. Fig. 6b shows the same plot for a shorter time range without data from the 1.4 V studies. The

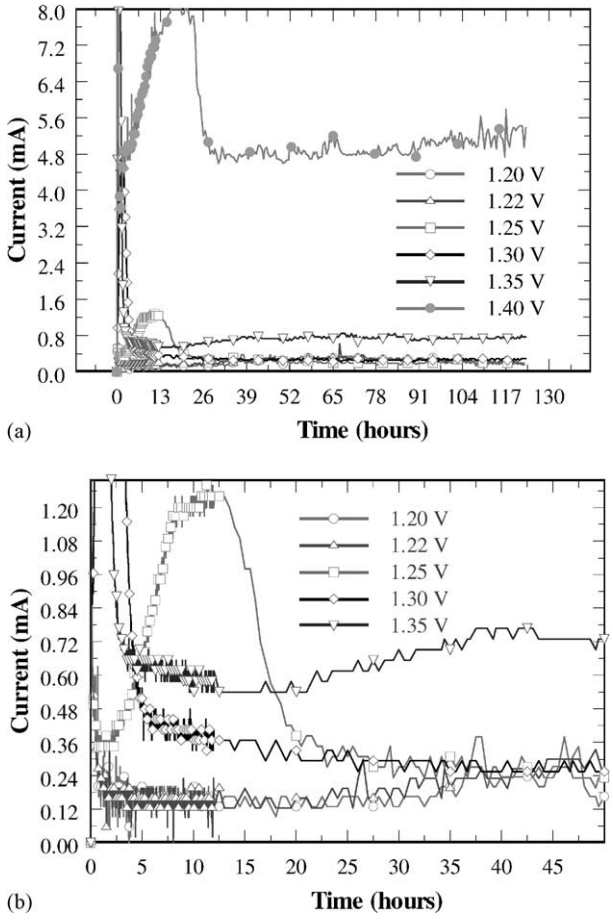

Fig. 6. Current as a function of time for different applied potentials for Pb–Sn alloy.

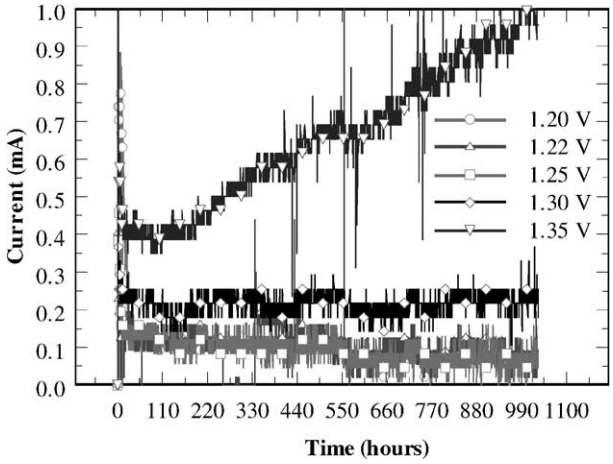

Fig. 7. Current as a function of time for different applied potentials for Pb–Sn–Ca alloy.

plot shows that the current remains at a minimum value for applied potentials of 1.2 and 1.22 V. At 1.25 V, the current initially increases then decreases and reaches a steady-state value closer to that seen for 1.3 V. The current at 1.35 and 1.4 V are much larger due to oxygen evolution becoming significant. Visual observation indicated that the surface became black for applied potentials of 1.25 V and beyond. At 1.20 and 1.22 V, the surface retained its initial color even after 6 weeks of testing. From Table 1, it is clear that below 1.2 V, PbO_2 is converted to $PbSO_4$. Hence, for this alloy a 50 mV overvoltage is needed for formation of the stable oxide film. After dissolution studies, the samples were washed with DI water and weighed.

Fig. 7 shows the change in current with time for the Pb–Sn–Ca alloy at different applied potentials. The values for 1.4 V are not included since oxygen evolution is the dominant reaction here and most of the current goes for O_2 generation. The behavior is similar to that of the Pb–Sn alloy. The plot shows that the current remains at a minimum value for applied potentials less than 1.25 V. Beyond 25 h no change in the corrosion current with time is seen for applied potentials lesser than 1.35 V. At 1.35 V, a steady increase in current with time is seen. This indicates that oxide film is unstable in this potential range. The studies were done for a time of 6 weeks. Fig. 7 shows the same plot for a shorter time range without data from the 1.35 V studies. At 1.25 V, the current initially increases then decreases and reaches a steady-state value closer to that seen for 1.3 V. Visual observation indicated that the surface became black for applied potentials of 1.25 V and beyond. After keeping the electrodes potentiostatically for 37 days, the Pb–Sn–Ca samples were washed and weighed. The weight loss results are shown in Fig. 8. Results obtained for the Pb–Sn alloy are also shown for comparison.

Fig. 8 shows the loss in weight of Pb–Sn and Pb–Sn–Ca alloy after oxidizing at different potentials. In general the rate of Pb dissolution is lower for the Pb–Sn–Ca alloy as compared to that of Pb–Sn alloy. This reduction in dissolution can arise

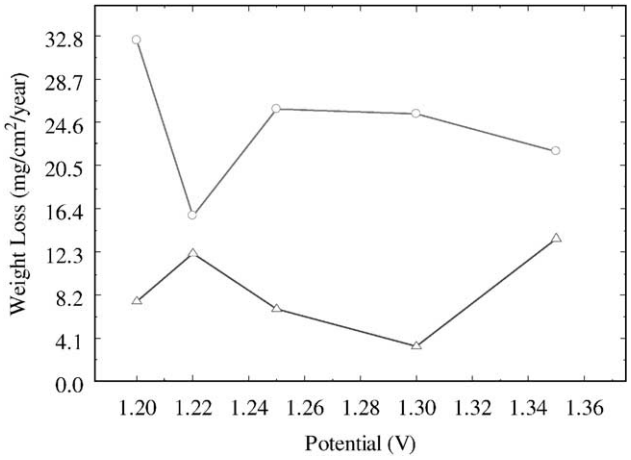

Fig. 8. Comparison of weight loss of Pb–Sn and Pb–Sn–Ca alloys after polarizing at different potentials.

either due to Ca addition or an increase in Sn content. The weight loss is at a maximum for 1.2 V. From Fig. 6b, it can be seen that the steady-state corrosion current is at a minimum at 1.2 V. The contradiction between the weight loss and potentiostatic oxidation studies arises due to the increase in the rate of oxygen evolution. At 1.2 V most of the current goes for alloy dissolution. At higher potentials, a larger fraction of the current goes towards oxygen evolution. Further, at 1.2 V, PbO_2 is converted to $PbSO_4$ which subsequently dissolves in the electrolyte. Hence, the weight loss is higher at 1.2 V. The corrosion is at a minimum at 1.22 V. Beyond this no change in the corrosion rate is seen from both the weight loss and potentiostatic studies.

3.4. Impedance analysis of Pb–Sn and Pb–Sn–Ca alloys

Electrochemical impedance spectroscopy (EIS) is a steady-state technique that can be used to study the oxide film on the surface. The impedance results for both alloys are shown in Fig. 9. The impedance data generally covers a frequency range from 0.1 Hz to 100 kHz with an ac voltage signal varying by ±5 mV, which ensures that the electrode system is under minimum perturbation. The potential perturbation was applied under various bias voltages. Prior to applying the sinusoidal signal, the electrode was held constant at the bias voltage for 15 min. This was done to maintain steady-state conditions during the actual impedance analysis. As seen from the plot, the resistance at low bias voltages (<1.18 V) is large. At this potential the passive film is still present on the electrode surface. Increasing the bias voltage results in dissolution of the passive film. At potentials above 1.2 V, $PbSO_4$ is converted to PbO_2. For potentials greater than 1.18 V, the Nyquist plots overlap over one another. The imaginary part of the impedance increases with decrease in frequency indicating that the reaction takes place actively on the surface. At potentials greater than 1.35 V, a semi-circle corresponding to oxygen reduction appears. In general it is clear that on both alloys no thick

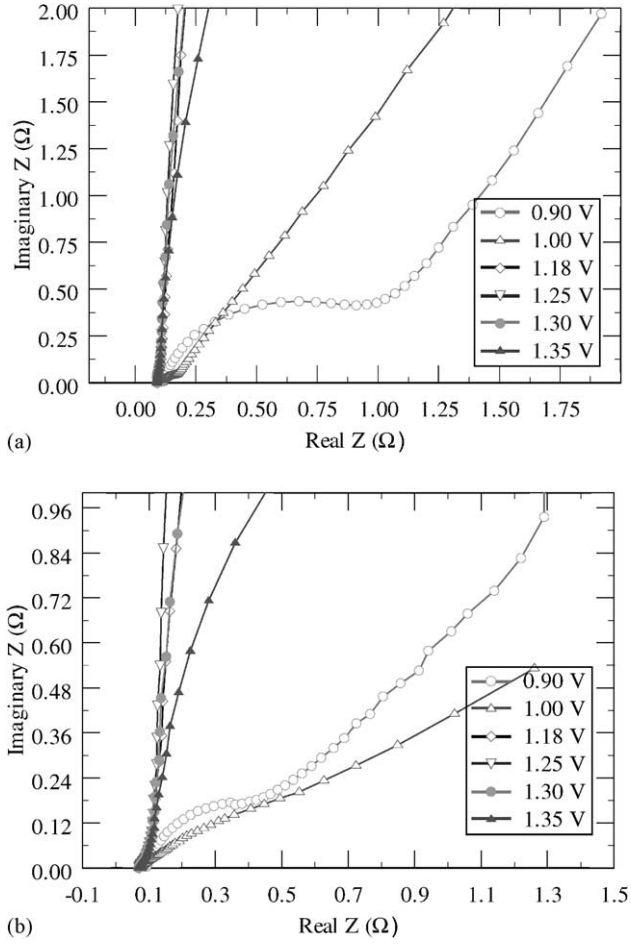

Fig. 9. Impedance analysis of Pb–Sn (a) and Pb–Sn–Ca (b).

oxide film is formed. Hence addition of Sn aids in the dissolution of the passive film.

3.5. Studies on Sn coated Pb electrodes

The studies above clearly show that doping Sn within lead anodes leads to the formation of a more conductive oxide film. The studies also show that the reversibility of the electrode is dependent on the surface film and not on the bulk material. One of the goals in lead acid cells is to increase the energy density without compromising on the charge–discharge efficiency after storage. Localizing Sn on the surface of the electrode rather than doping it in the bulk of the material can solve the problem of alloy reversibility and also decrease the weight of the electrode. To accomplish this, Sn was electrodeposited on the lead anode. Varying the time of deposition one can control the thickness of the coating. Fig. 10a and b presents the scanning electron micrographs of Pb–Sn alloy and Sn coated Pb, respectively. Both the surfaces are porous in nature indicating that electrolyte can easily penetrate the oxide film and reach the underlying substrate. This is critical to maintain reversibility after long periods of storage. The Pb–Sn alloy shows

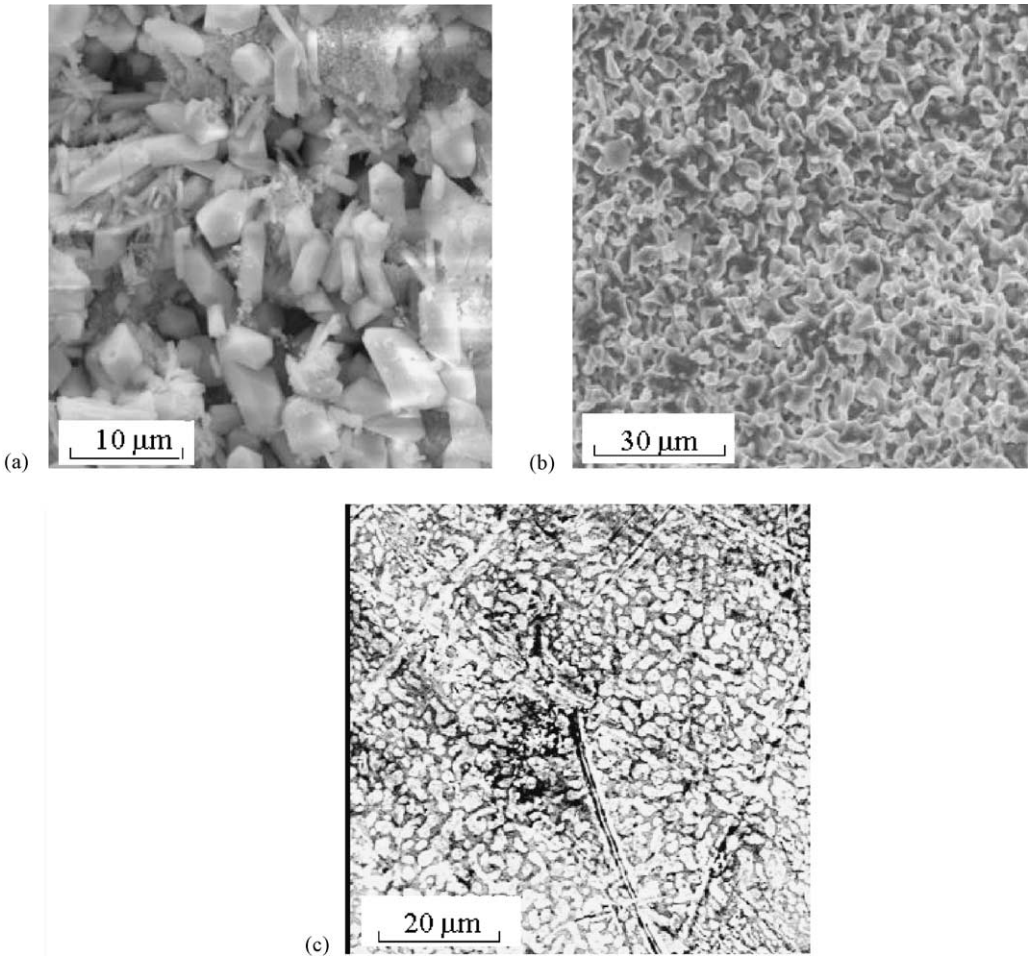

Fig. 10. Scanning electron micrographs of Pb–Sn alloy (a), Sn coated Pb (b), and tin coated Pb subjected to quenching (c).

the presence of cylindrical nodules on its surface. Closer examination reveals that the size of these particles is in the range of 2 microns. After anodic oxidation of the Pb–Sn alloy (not shown), the size of the nodules does not change. The surface remains porous causing the surface oxide film to remain conductive. Coating Pb with Sn leads to a two-dimensional networked porous structure as seen in Fig. 10b. Initial corrosion studies indicate that the rate of Pb dissolution remains high in this case due to the highly porous nature of the surface film. In this case, it was found that the oxidation rate is much higher as compared to that of Pb–Sn and Pb–Sn–Ca alloys. While it is desirable to have a porous oxide film, higher rates of dissolution will result in low cycle life and high capacity fade with cycling. In order to reduce the porosity of the film the coated material was quenched in Thermanol oil at 300 °C for 30 s. Tin melts at 231.93 °C and Pb melts at 327.46 °C. Heating the coating at 300 °C leads to the melting of Sn and formation of a eutectic melt with Pb. Fig. 10c presents the micrograph of the surface after quenching in Thermanol oil. SEM analysis reveals that subsequent to quenching the deposit becomes less porous in nature with a mixture of Sn and Pb covering the surface.

Subsequent to deposition potentiodynamic and cyclic voltammetry studies were done on the coated electrodes. The potentiodynamic profile reveals that the anode characteristics remain similar to that of Pb–Sn and Pb–Sn–Ca alloys. Fig. 11 presents the cyclic voltammograms of Sn coated Pb anode after quenching. The potential was swept from 0.6 to 1.4 V and then back to 0.6 V at a scan rate of 50 mV/s. Analysis of the CVs of Sn coated Pb anode show that the behavior is similar to that of Pb–Sn and Pb–Sn–Ca alloys. Initial cycling does not reveal any reduction peaks. Since the deposited Sn and surface Pb are not oxidized, initial cycling leads to the formation of Sn oxide and PbO_2. Once a stable surface film is formed reduction peaks are seen after 400 cycles. Further cycling leads to a more reversible behavior. Table 2 presents the peak current, peak potential and reversible potentials for the Sn coated anode. After 1500 cycles the peak potential appears at 1.14 V. This value is slightly more positive than that seen for Pb–Sn and Pb–Sn–Ca alloys as shown in Table 1. As mentioned before, the increase in peak current is directly dependent on the amount of Sn present on the surface. In this case, the peak current values lie close to that of Pb–Sn–Ca with 1.1% Sn and are

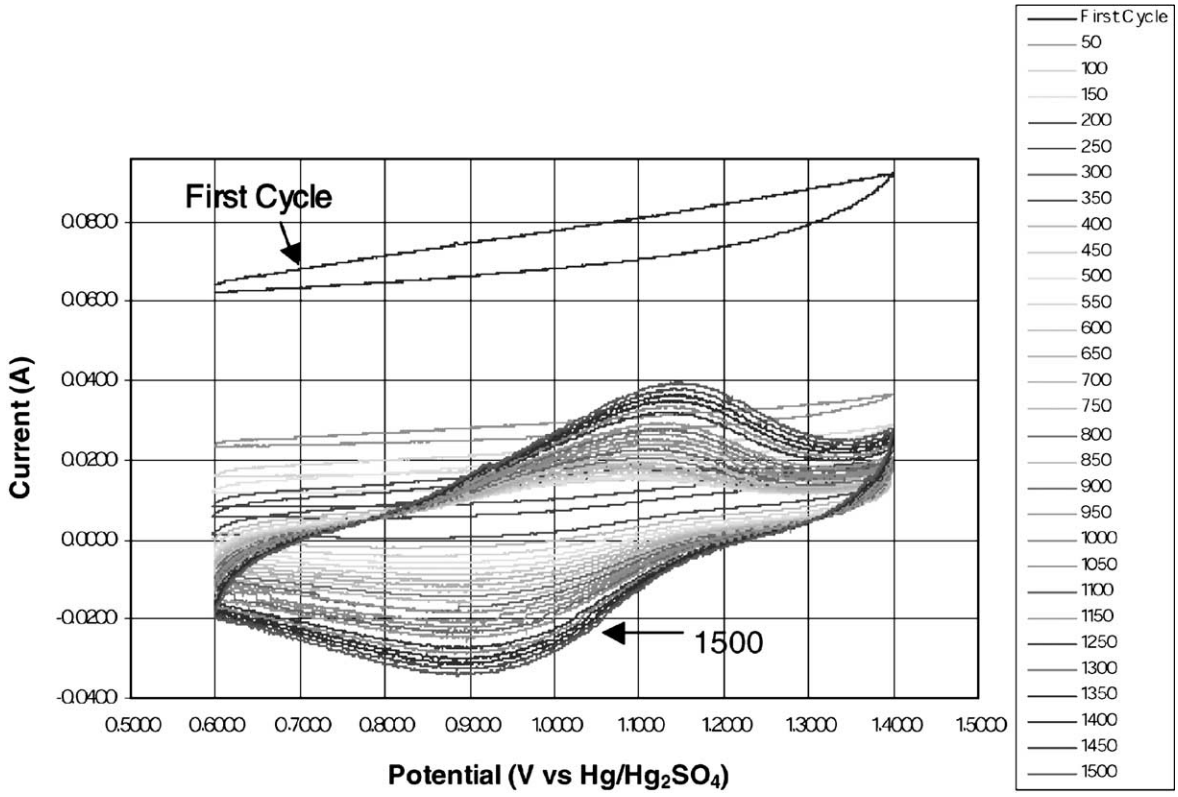

Fig. 11. Cyclic voltammograms of Sn coated Pb electrode in 30% sulfuric acid. The alloy was quenched before immersing in sulfuric acid. The scan rate was 50 mV/s.

larger than that of the Pb–Sn alloy with 0.6% Sn. Further, the peak oxidation current increases with cycling. Between cycles 500 and 900 the increase is 45% and between cycles 1100 and 1500 the increase is 41%. These results clearly show that deposition of Sn aids in dissolution of the passive film and increases the reversibility of the anodic reaction. The last column in Table 2 presents the potential at which current becomes negative during the reverse sweep. This corresponds to the reduction of PbO_2 to $PbSO_4$. After 1500 cycles, this potential is around 1.2 V for the Pb–Sn alloy and 1.24 V for the Pb–Sn–Ca alloy. For the Sn coated electrode, this potential is around 1.23 V, which is closer to that of the Pb–Sn–Ca alloy. As mentioned before, when applying a float voltage to the positive electrode, in order to keep it in the oxidized state the value should be more positive than 1.20 V. Next dissolution studies were done to determine the rate of Sn loss from the coated electrode.

Table 2
Change in peak current, peak potential and reversible potential for Sn coated Pb

Cycle number	Peak current (mA)	Peak potential (V)	$E_{rev,f}$ (V)	$E_{rev,b}$ (V)
400	15.1	1.396	0.600	1.010
500	15.7	1.090	0.617	1.088
750	19.2	1.080	0.653	1.156
900	22.8	1.140	0.668	1.176
1100	28.0	1.120	0.682	1.199
1250	32.0	1.140	0.692	1.213
1500	39.4	1.140	0.704	1.231

The alloy dissolution studies were done at different float potentials. Fig. 12 presents the change in current as a function of time. The values for 1.4 V are not shown since the currents are large due to oxygen evolution. The current initially is high and subsequently decreases except for a float

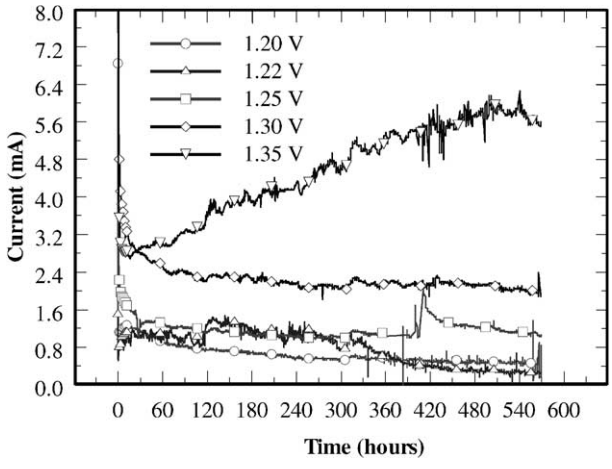

Fig. 12. Current as a function of time for different applied potentials for Sn coated Pb electrode. The electrode was quenched before corrosion testing.

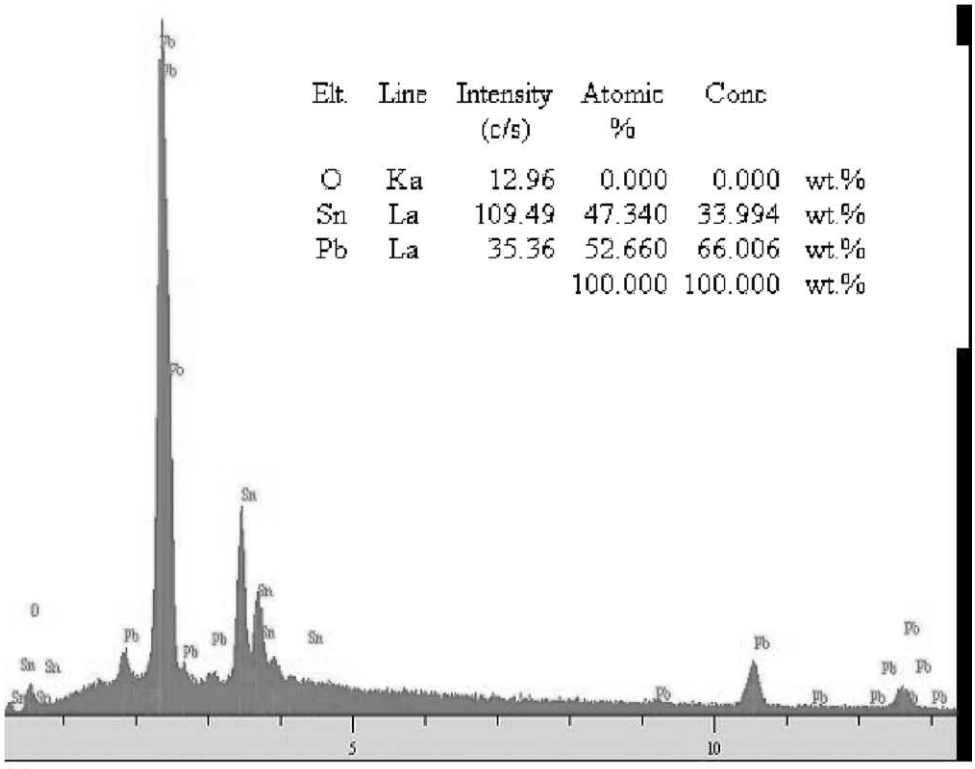

(a)

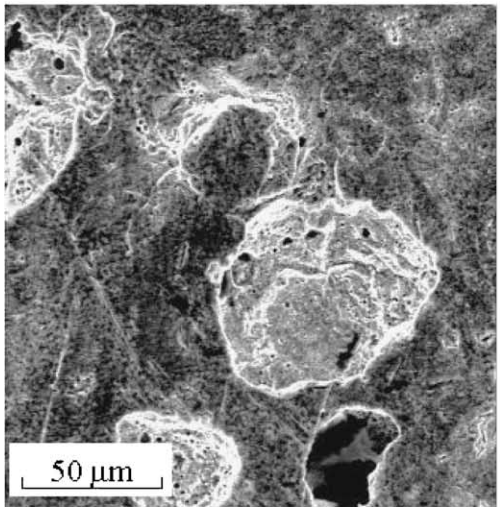

(b)

Fig. 13. EDAX (a) and SEM (b) analysis of Sn coated electrode. The electrode was kept at a float potential of 1.25 V.

voltage of 1.35 V. In this case, the current keeps increasing indicating high rate of metal dissolution or oxygen evolution. The currents remain at the same value for float potentials of 1.2–1.25 V. Comparing the magnitude of the corrosion currents in Fig. 12 with that for Pb–Sn and Pb–Sn–Ca alloys in Figs. 6 and 7, it can be seen that electrodeposited Sn shows similar behavior as Sn doped alloys. After a period of 6 weeks, the samples were taken from solution and washed with DI water. Subsequently, surface analysis was done to determine the morphology and constituents on the surface layer.

Fig. 13 presents the EDAX and SEM analysis after 6 weeks of corrosion testing for the Sn coated sample kept at 1.25 V. EDAX shows that Sn is still present on the surface. After quenching the amount of Sn present on the surface was 54 wt.%. The same sample after 6 weeks of corrosion testing at 1.2 V has 34 wt.% Sn. Further, the surface morphology as shown in Fig. 13b indicates that the surface remains porous in nature. It is also seen that white precipitates of oxidation products are formed on the surface. The exact nature of the surface film formed is not clear. Further studies need to be done to determine the changes in the composition of oxide

film as a function of float voltage and storage time. In general, these results show that electrodeposition of Sn on Pb offers an inexpensive route to improving the charging efficiency and reversibility of Pb anodes in lead acid batteries.

4. Conclusions

This paper presents an evaluation of Sn doping and its effect on the reversibility of Pb anodes used in lead acid batteries. Potentiodynamic studies reveal that an oxide film is formed on the surface of Pb–Sn alloys over a wide range of potentials. However, this oxide film is non-porous in nature and does not inhibit the charging efficiency of the anode. Cyclic voltammograms of Pb–Sn and Pb–Sn–Ca alloys show that the oxidation current increases with repeated cycling. This result is in opposite to that seen in pure lead anodes where the oxidation current decreases with cycling. Hence, it is clear that addition of Sn aids in making the surface film more conductive thereby allowing the electrolyte to reach the underlying lead grid. Float potential studies on Pb–Sn and Pb–Sn–Ca alloys show that both the alloy dissolution and oxygen evolution are at a minimum between 1.2 and 1.25 V. Beyond 1.25 V, the rate of oxygen evolution increases while the metal dissolution remains the same. For lead acid cells stored under float voltages greater than 1.25 V electrolyte loss due to oxygen evolution could be of serious concern. Finally, it has been shown that electrodeposition of Sn on lead can offer similar advantages as doping Sn into lead. Through the use of a thermal treatment procedure the rate of anode dissolution has been minimized while maintaining the high reversibility and charging efficiency of the anode.

Acknowledgements

Authors acknowledge financial support by NorthStar Battery Company.

References

[1] Z. Takehara, J. Power Sources 85 (2000) 29.
[2] J. Burbank, J. Electrochem. Soc. 106 (1959) 369.
[3] B. Culpin, A.F. Hollenkamp, D.A.J. Rand, J. Power Sources 38 (1992) 63.
[4] R.F. Nelson, D.M. Wisdom, J. Power Sources 33 (1991) 165.
[5] E. Hameenoja, T. Laitinen, G. Sundholm, A. Yli-Pentti, Electrochim. Acta 34 (1989) 233.
[6] F.A. Fleming, G.J. May, X. Muneret, White Paper on the Use of Lead–Tin Alloys in VRLA Batteries for Extreme Telecommunication Applications.
[7] I. Petersson, E. Ahlberg, J. Power Sources 91 (2000) 143.
[8] H.K. Giess, in: K.R. Bullock, D. Pavlov (Eds.), Proceedings of the Symposium on Advances in Lead–Acid Batteries, Vol. 84-14, The Electrochemical Society, Pennington, NJ, USA, 1984, p. 241.
[9] D. Pavlov, C.N. Poulieff, E. Klaja, N. Jordanov, J. Electrochem. Soc. 116 (1969) 316.
[10] K. Takahashi, N. Hoshihara, H. Yasuda, T. Ishii, H. Jinbo, J. Power Sources 30 (1999) 23.
[11] B.J. Carter, S.D. Stefano, L. Whitcanack, Ext. Abstr. No. 94, Vol. 86-2, The Electrochemical Society, Pennington, NJ, USA, 1986, p. 133.
[12] R.F. Nelson, D.M. Wisdom, J. Power Sources 33 (1991) 165.